

# Temporal Progressive Attention for Early Action Prediction

Alexandros Stergiou and Dima Damen

Department of Computer Science, University of Bristol, UK  
{alexandros.stergiou, dima.damen}@bristol.ac.uk

**Abstract.** Early action prediction deals with inferring the ongoing action from partially-observed videos, typically at the outset of the video. We propose a bottleneck-based attention model that captures the evolution of the action, through progressive sampling over fine-to-coarse scales. Our proposed **Temporal Progressive** (TemPr) model is composed of multiple attention towers, one for each scale. The predicted action label is based on the collective agreement considering confidences of these attention towers. Extensive experiments over three video datasets showcase state-of-the-art performance on the task of Early Action Prediction across a range of backbone architectures. We demonstrate the effectiveness and consistency of TemPr through detailed ablations. <sup>1</sup>

## 1 Introduction

Early action prediction (EAP) is the task of inferring the action label corresponding to a given video, from only partially observing the start of that video. Interest in EAP has increased in recent years due to both the ever-growing number of videos recorded and the requirement of processing them with minimal latency. Motivated by the advances in action recognition [6,56], where the entire video is used to recognize the action label, recent EAP methods [3,15,33,44,59] distill the knowledge from these recognition models to learn from the observed segments. Despite promising results, the information that can be extracted from the partial and full videos is inevitably different. We instead focus on modeling the observed partial video better.

Several neurophysiological studies [11,28] have suggested that humans understand actions in a predictive and not reactive manner. This has resulted in the *direct matching hypothesis* [17,45] where, actions are believed to be perceived through common patterns. Encountering any of these patterns prompts the expectation of specific action(s), even before the action is completed. Although the early prediction of actions is an inherent part of human cognition, the task remains challenging for computational modeling.

Motivated by the direct matching hypothesis, we propose a Temporally Progressive (TemPr) approach to model partially observed videos. We represent the observed video by a set of sub-sequences of temporally increasing lengths,

---

<sup>1</sup> Code is available at: <https://github.com/alexandrosstergiou/progressive-action-prediction>

which we refer to as video scales, inspired by multi-scale representations in images [8,67] and video [26,61]. TemPr uses distinct stacks of transformer blocks, that we define as towers, over each input video scale. These utilize a shared latent-bottleneck for cross-attention [27,36], followed by a stack of self-attention blocks to concurrently encode and aggregate the input. From the tower outputs, a shared classifier produces label predictions for each scale. An adaptive accumulation function then predicts action labels based on the similarity between tower predictors and the confidence of individual predictors.

In summary, our contributions are as follows: (i) We propose a progressive fine-to-coarse sampling approach for EAP. (ii) We use transformer towers over sampled scales to capture discriminative representations. (iii) We utilize an adaptive accumulation function for the aggregation of predictions from each attention tower, based on their confidence and collective agreement. (iv) We evaluate the effectiveness of our approach over UCF-101 [52], NTU-RGB [50] and Something-Something (sub-21 & v2) [20] video datasets.

## 2 Related Work

The task of EAP is distinctly different from, but related to, the tasks of action recognition and action anticipation. EAP predicts the *ongoing* action label while only observing the first part of the video. In contrast, recognition assumes the *completed* action has been fully observed, while anticipation forecasts potential *upcoming* actions, with decisions made seconds before the action starts. We first review prior EAP approaches, before relating our method to those used for related video understanding tasks.

**Early action prediction:** Most of the early attempts have focused on the probabilistic modeling of partially observed videos [4,35,37,38,46]. For example, Ryoo *et al.* [46] used a bag-of-words approach to model feature distributions over multiple partially observed videos. Later approaches aimed to overcome errors where large appearance variations occur, by either sparse coded feature bases [4] or through a scoring function [30,32], combining prior knowledge and the sequential order of frames. Lan *et al.* [35] studied the representation of movements within the partially observed video, using a hierarchical structure.

More recent methods [3,15,24,25,31,59,63,65,69] have used learnt-features. Specifically, knowledge distillation [23,43] has been used to transfer class knowledge from the full videos to their corresponding partial videos. This was achieved using Long Short-Term Memory (LSTM) models [25,42,59] and teacher-student frameworks [3,15,59]. Other methods have been based on recurrent architectures with additional memory cells [31] for matching similar characteristics from the full and partial videos. Xu *et al.* [65] proposed a Conditional Generative Adversarial Network (CGAN) to generate feature representations for the entire video, from the partially observed video. Approaches have also focused on the propagation of residual features [69] or human-object interactions exploration with graph convolutions through relation reasoning [62,63].

In contrast, we hypothesize that it is more beneficial to focus on better representations of the partial video solely. Our method is based on sampling at varying-length scales from the observed video to understand the temporal progression of actions. We show that this strategy, combined with aggregating tower predictors, can lead to notable improvements in accuracy. We are the first to study EAP in this progressive manner.

**Multi-scale representations for other video understanding tasks.** The usage of scales, i.e. sequences of varying lengths or sampling at differing rates, has varied depending on the video understanding task [16,19,41,49,64,70,71]. For action recognition, video scales have been primarily used as a sampling method for either relational reasoning [14,49,71] or to select the most salient scale(s) as input to the network [41,64,70]. In action anticipation, methods utilize different scales to combine features from video snippets and anticipate one or more upcoming actions [16,19]. Different from these tasks, we propose to utilize progressive video scales, which capture fine-to-coarse representations making them more suitable for partially observed videos.

**Attention for video tasks.** Attention-based video methods [58,60] have initially been used as part of spatio-temporal CNN architectures [6,56]. The recent introduction of Vision Transformer [10], has inspired subsequent works on action recognition by either focusing on how spatio-temporal information can be processed [1,2] or architectural optimizations for spatio-temporal data [12,39,47,66,68]. Motivated by the recent advances of spatio-temporal transformers for action recognition, we combine multiple transformer towers in our TemPr model.

### 3 Our Approach

In this section, we overview our TemPr model (shown in Fig. 1). We first introduce our prime contribution of progressive scales for sampling from the observed video in Section 3.2. Each scale corresponds to an attention tower, which captures the progression of the action, and predicts the ongoing action, as explained in Section 3.3. Multiple scales/towers are then combined for a final prediction by an accumulation function, detailed in Section 3.4.

#### 3.1 Early Action Prediction (EAP): Problem definition

We follow the definition of the EAP task from recent works [3,63,65,69]. We denote the full video with  $T$  frames as  $\mathbf{v}_{\{1,\dots,T\}}$ . We define the *observation ratio*  $0 < \rho < 1$  as the proportion of frames observed. EAP assumes  $0 < \rho$ , i.e. at least one frame of the video depicting the action has been observed, and  $\rho < 1$ , so part of the video remains unobserved. Accordingly,  $T_\rho = \lceil \rho \cdot T \rceil$  is the number of observed frames. In EAP, the prediction of the ongoing action label  $y$  conveyed in the full video  $\mathbf{v}_{\{1,\dots,T\}}$  is attempted from only the observed  $T_\rho$  frames.

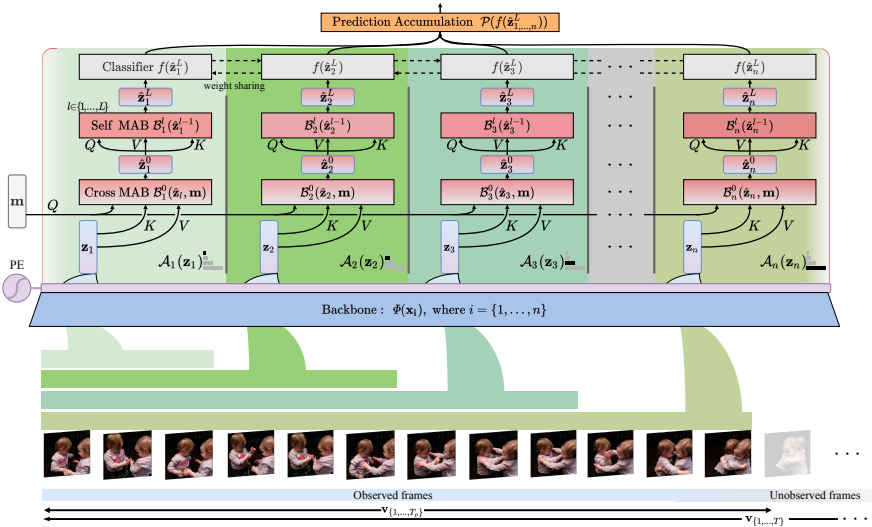


Fig. 1: **TemPr**. Features are extracted over each input  $\mathbf{x}_i$  sampled from video scale  $\mathbf{s}_i$ , and combined with scale and spatio-temporal positional encodings (PE). The feature volumes  $\mathbf{z}_i$  are passed to attention towers that utilize a shared latent array  $\mathbf{m}$  for their cross-attention block (Cross MAB). This is followed by a stack of  $L$  self-attention blocks (Self MAB) to output feature tensors  $\hat{\mathbf{z}}_i^L$  in the latent space. Shared-weight classifier  $f(\cdot)$  is applied to every tower output to make per-scale predictions. These predictions are aggregated by the accumulation function  $\mathcal{P}(\cdot)$  for early action prediction over the observed frames.

### 3.2 Temporal progressive video scales

Given the partial observation of the action, we speculate that the sampling strategy is critical to capture distinctive representations of the ongoing action. This is different from the sampling typically utilized in action recognition, where the video is uniformly split into equally-sized segments [57]. Equal-sized segments, in partially observed videos, can miss the discriminative action pattern when this pattern spans across segments. We thus propose to sample at multiple scales within the observed video, which we refer to as *progressive* sampling.

Given the partially observed video of  $T_\rho$  frames, we examine the ongoing action over  $n$  scales  $\mathbf{s}_{\{1, \dots, n\}}$ . Each scale  $\mathbf{s}_i$  has a larger temporal length to sample from than  $\mathbf{s}_{i-1}$ . We represent each scale  $\mathbf{s}_i$  as:

$$\mathbf{s}_i = \{1, \dots, T_{\mathbf{s}_i}\}, \text{ where } T_{\mathbf{s}_i} = \frac{i}{n} \cdot T_\rho \quad \forall i \in \mathbf{N} = \{1, \dots, n\} \quad (1)$$

Over each scale, we sample  $F$  frames randomly to capture a progressive fine-to-coarse representation of the video. Considering the difference in input length per scale, sampling a fixed number of frames,  $F$ , is also required in order to standardize the backbone inputs. An illustration of our video scales sampling

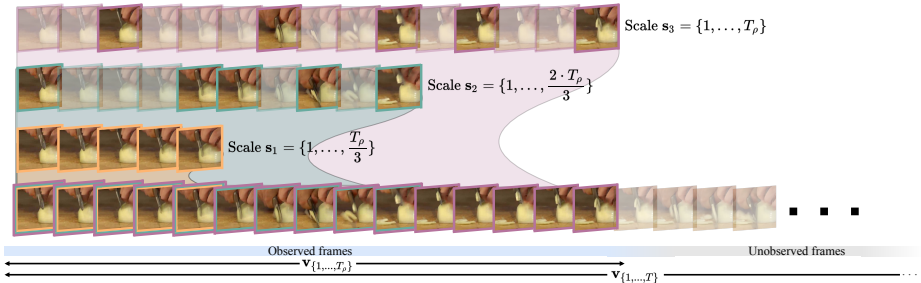


Fig. 2: **Progressive video scale sampling.** The observed video sequence (bottom) is represented by  $n = 3$  scales. The temporal length of each scale increases progressively (a)  $T_{\mathbf{s}_1} = \frac{1}{3} \cdot T_\rho$ , (b)  $T_{\mathbf{s}_2} = \frac{2}{3} \cdot T_\rho$  and (c)  $T_{\mathbf{s}_3} = T_\rho$ . The randomly sampled frames  $F = 5$  from each scale are highlighted.

approach can be seen in Fig. 2, in which  $n = 3$  scales are depicted, with  $F = 5$  frames sampled per-scale.

### 3.3 Temporal Progressive Attention Towers

We use a shared backbone  $\Phi(\cdot)$  to extract features from the sampled frames, over the progressive scales. Corresponding to each scale  $\mathbf{s}_i$ , we define input volume  $\mathbf{x}_i$  of size  $3 \times F \times H \times W$ , with  $F$  temporally ordered frames,  $H$  height and  $W$  width. We thus define  $\mathbf{z}_i = \Phi(\mathbf{x}_i)$  to be the per-scale, multi-dimensional spatio-temporal feature volume, of size  $C \times t \times h \times w$ . The spatio-temporal features are further down-scaled with average pooling, to ensure a fixed size  $t \leq F$ ,  $h \ll H$  and  $w \ll W$ . Given the scales' spatio-temporal features  $\mathbf{z}_1, \dots, \mathbf{z}_n$ , we reshape these to  $C \times (thw)$ , and concatenate Fourier Positional Embeddings (PE) of size  $n \times (thw)$  to encode each scale and space-time position. Features  $\mathbf{z}_i$  form the input to attention tower  $\mathcal{A}_i$ .

We attend over each scale's features using a corresponding attention tower,  $\mathcal{A}_1, \dots, \mathcal{A}_n$ , so that  $\hat{\mathbf{z}}_i^L = \mathcal{A}_i(\mathbf{z}_i)$ , where  $\hat{\mathbf{z}}_i^L$  is the feature volume after attending to the input volume  $\mathbf{z}_i$  over the transformer blocks.

Motivated by the recent architectural approaches for dealing with the quadratic scaling of complexity in transformers [27,36], each tower uses two attention components consisting of one cross-attention block and a stack of self-attention blocks followed by a shared predictor. Attention blocks are indexed by  $l \in \{0, \dots, L\}$  and towers are indexed by  $i \in \mathbf{N}$ . We describe these components next.

**Cross Multi-Head Attention Block** (Cross MAB), employs a latent array  $\mathbf{m}$  of  $D \times d$  size ( $d \ll thw$ ), where  $D$  is the transformer latent space size. This latent array is used to create an asymmetric query-key-value (**QKV**) attention function in which  $\mathbf{Q} \in \mathbb{R}^{D \times d}$ ,  $\mathbf{K} \in \mathbb{R}^{C \times (thw)}$ ,  $\mathbf{V} \in \mathbb{R}^{C \times (thw)}$ . The Cross MAB block  $\hat{\mathbf{z}}_i^0 = \mathcal{B}_i^0(\mathbf{z}_i, \mathbf{m})$  consists of a Multi-Head Cross Attention (MCA), a Layer Normalization (LN) and a Multilayer Perceptron (MLP) module:

$$\begin{aligned}\widehat{\mathbf{z}}_i^0 &= MLP_i^0(LN(\mathbf{h}_i^0)) + \mathbf{h}_i^0, \text{ where} \\ \mathbf{h}_i^0 &= MCA_i^0(LN(\mathbf{m}), LN(\mathbf{z}_i)) + \mathbf{m} \quad \forall i \in \mathbf{N}\end{aligned}\quad (2)$$

in which, the MCA operation computes the dot-product attention of tensors  $\mathbf{m}$  and  $\mathbf{z}_i$ , where  $\mathbf{m}$  forms the query and  $\mathbf{z}_i$  forms the keys and values.

**Stacked Self-Attention Blocks** (Self MAB), correspond to a stack of  $L$  transformer blocks [10], symmetrically attending to tensors  $\widehat{\mathbf{z}}_i^l \forall l \in \{0, \dots, L-1\}$ . Based on Multi-Head Self Attention (MSA), each transformer block  $\widehat{\mathbf{z}}_i^l = \mathcal{B}_i^l(\widehat{\mathbf{z}}_i^{l-1})$  is denoted as:

$$\begin{aligned}\widehat{\mathbf{z}}_i^l &= MLP_i^l(LN(\mathbf{h}_i^l)) + \mathbf{h}_i^l, \text{ where} \\ \mathbf{h}_i^l &= MSA_i^l(LN(\widehat{\mathbf{z}}_i^l)) + \widehat{\mathbf{z}}_i^{l-1} \quad \forall i \in \mathbf{N}, l \in \{1, \dots, L\}\end{aligned}\quad (3)$$

By exploiting the bottleneck from Cross MAB [27], the transformer towers are significantly more efficient than a sole deep stack of self-attention blocks. The use of a latent vector, of parameterizable size, can benefit the creation of balanced models in terms of performance, minimizing feature redundancies.

**Attention tower predictors.** Towers additionally include a linear classifier  $f(\widehat{\mathbf{z}}_i^L)$  that maps the output  $\widehat{\mathbf{z}}_i^L$  to the set of  $\mathbf{Y}$  classes. Classifier weights are shared across scales, to predict action class label  $\widehat{y}$ . As features  $\widehat{\mathbf{z}}_i^L$  are bound to their video scale  $\mathbf{s}_i$ , towers cannot discover feature relationships across different scales. This limits their modeling capabilities. By sharing weights over their linear classifiers, a joint feature space is established.

### 3.4 Accumulation Function for EAP

Predictions from multiple scales represent fine-to-coarse class predictions. We wish to accumulate the individual scale predictions, while acknowledging that different scales can be more descriptive for specific video instances.

In order to deal with the identified limitations of individual predictors, we introduce an aggregation function  $\mathcal{P}(f(\widehat{\mathbf{z}}_i))$  for accumulating tower predictions<sup>2</sup>. The function is formulated based on the agreement between predictions and the individual towers' confidence in the produced prediction.

**Predictor agreement** aims to combine individual predictions by focusing on their agreement. We formulate this based on the assumption that predictions with high degree of resemblance, in terms of their class probability distribution, can reduce the uncertainty of individual predictors. We utilize Exponential Inverse Coefficient Weighting ( $eICW$ ) [53] for the weighted aggregation of probability distributions  $f(\widehat{\mathbf{z}}_i)$  of each scale, based on their similarity to the mean class probability distribution  $\overline{f(\widehat{\mathbf{z}})} = \frac{1}{n} \sum_{i \in \mathbf{N}} f(\widehat{\mathbf{z}}_i)$ . This aims to reduce the effect of outlier predictions that are geometrically further from the mean prediction. Distributions that are closer to the mean are accordingly weighted higher:

<sup>2</sup> To improve clarity, we refrain from denoting the attention layer index  $l$ , since all predictions are made based on the final attention block output  $\widehat{\mathbf{z}}_{1, \dots, n}^L$  of each tower.

$$\mathcal{P}_{eICW}(f(\widehat{\mathbf{z}}_i), \overline{f(\widehat{\mathbf{z}})}) = \sum_{i \in \mathbf{N}} \frac{e^{DSC(f(\widehat{\mathbf{z}}_i), \overline{f(\widehat{\mathbf{z}})})^{-1}} \cdot f(\widehat{\mathbf{z}}_i)}{\sum_{k \in \mathbf{N}} e^{DSC(f(\widehat{\mathbf{z}}_k), \overline{f(\widehat{\mathbf{z}})})^{-1}}} \quad (4)$$

in which  $DSC(\cdot)$  is the Dice-Sørensen coefficient [9] between class probabilities  $f(\widehat{\mathbf{z}}_i)$  and the mean class probabilities  $\overline{f(\widehat{\mathbf{z}})}$  for every  $y$  of all  $\mathbf{Y}$  labels:

$$DSC(f(\widehat{\mathbf{z}}_i), \overline{f(\widehat{\mathbf{z}})}) = \sum_{y \in \mathbf{Y}} \frac{2 \cdot \|f(\widehat{\mathbf{z}}_i)_y \cdot \overline{f(\widehat{\mathbf{z}})}_y\|}{\|f(\widehat{\mathbf{z}}_i)_y\| + \|\overline{f(\widehat{\mathbf{z}})}_y\|} \quad (5)$$

**Predictor confidence** is used to aggregate predictions from individual scales based on the sharpness of their probability distribution. We calculate the exponential maximum (i.e. softmax) over all predictions. Predictions that demonstrate high class probability for a single or a small set of classes are weighted higher than predictions with probability distributions that are closer to uniform:

$$\mathcal{P}_{eM}(f(\widehat{\mathbf{z}}_i)) = \sum_{i \in \mathbf{N}} \frac{e^{f(\widehat{\mathbf{z}}_i)} \cdot f(\widehat{\mathbf{z}}_i)}{\sum_{k \in \mathbf{N}} e^{f(\widehat{\mathbf{z}}_k)}} \quad (6)$$

We use a combination of the two prediction aggregation strategies to create the final adaptive predictor accumulation function  $\mathcal{P}(f(\widehat{\mathbf{z}}_i))$ . As in [53], we use a dedicated parameter  $0 \leq \beta \leq 1$ , which we learn during training, to determine the proportion from each method:

$$\mathcal{P}(f(\widehat{\mathbf{z}}_i)) = \beta \cdot \mathcal{P}_{eICW}(f(\widehat{\mathbf{z}}_i), \overline{f(\widehat{\mathbf{z}})}) + (1 - \beta) \cdot \mathcal{P}_{eM}(f(\widehat{\mathbf{z}}_i)) \quad (7)$$

We refer to this aggregation function as our proposed *adaptive* accumulation function for attention tower predictions.

During training, we use the adaptive probability distribution from  $\mathcal{P}(f(\widehat{\mathbf{z}}_i))$  to calculate the divergence from the target one-hot categorical distribution for class vector  $\mathbf{y}$ . In inference, the arg max class is used as the EAP label.

## 4 Experiments

The datasets used, alongside implementation and training scheme details, are explained in Section 4.1. We include comparisons over state-of-the-art models in Section 4.2. We follow with ablation studies on model configurations over UCF-101 in Section 4.3. Finally, we include results on the large-scale Something-Something v2 dataset [20], presenting the first large-scale benchmark for EAP, in Section 4.4.

## 4.1 Datasets and Implementation details

**Datasets** We report our method’s performance over a diverse set of video datasets which have been previously used for EAP. *UCF-101* [52] consists of 101 classes and 13K videos in total. The dataset includes various types of human actions including human-object interactions, body-motions, human-human interactions, playing musical instruments and sports. The *Something-Something* (SSv1/SSsub21/SSv2) [20] is a collection of 100K (SSv1) & 220K (SSv2) videos of 174 fine-grained human-object action and interaction categories. The v1 of the dataset also includes a 21-action categories subset (SSsub21) of 11K videos used previously in [62,63] for EAP. We report on this subset, for direct comparisons. We also use the RGB-only version of *NTU RGB+D* [50] dataset, as in [33,37], containing 60 action classes and 57K videos of daily human actions.

**Model settings.** We evaluate our model over four scales  $n = \{1, 2, 3, 4\}$ . We use the concise visual notation:  $-$ ,  $=$ ,  $\underline{=}$ ,  $\underline{\underline{=}}$  to refer to these 4 configurations. Except during ablations, we follow model configurations similar to [27,36] for each attention tower ( $L = 8$ ,  $d = 256$ ,  $D = 512$ ,  $H_C = 4$ ,  $H_S = 8$ )<sup>3</sup>. Overall, we employ five different backbone architectures. MoViNet-A4 [29] is used as our main backbone across datasets in Section 4.2 due to its beneficial efficiency and high accuracy on action recognition. A 3D ResNet-18 with TemPr  $\underline{\underline{=}}$  is used for the ablation studies in Section 4.3. We additionally experiment with other widely used action prediction backbones ResNet-50 [21], ResNeXt-101 [21], X3D<sub>M</sub> [13] and (video) Swin-B [39]. All convolutional backbones have been originally pre-trained on Kinetics-700 [51] and then trained on each dataset over the full videos. Swin-B weights are initialized with the official model weights, pre-trained on Kinetics-600 [5]. We sample  $F = 16$  frames for each scale<sup>4</sup>. Backbones are used as feature extractors based on which we train TemPr on the partial videos.

**Training scheme.** For both UCF-101 and NTU-RGB, we process the videos by scaling the height to 384px and taking a center crop to size 384×384px followed by a random crop of 224×224px. Because of SSsub21’s low frame resolution, we scale the input frames to 100×176px. We initialize  $\beta$  with 0.5 and train for 60 epochs with base learning rate of  $1e^{-2}$  for TemPr and  $1e^{-3}$  for  $\beta$ . Both learning rates are reduced on epochs  $\{14, 32, 44\}$  by  $1e^{-1}$ . We use batch sizes of 32 for UCF-101, NTU-RGB & SSv2 and 64 for SSsub21 with AdamW &  $1e^{-5}$  weight decay.

## 4.2 Comparative results

We compare to state-of-the-art EAP methods across three datasets.

**UCF-101.** We divide prior methods based on their backbone architectures, and compare our model using standard [21] and more recent backbones [13,29], in Table 1. We demonstrate that our TemPr  $\underline{\underline{=}}$  model consistently outperforms

<sup>3</sup>  $L$  is the number of self-attention layers,  $d$  is the latent bottleneck,  $D$  is the latent channels,  $H_C$  and  $H_S$  are the numbers of cross and self-attention heads respectively.

<sup>4</sup> We use adaptive average pooling for down-scaling backbone output features  $\mathbf{z}_i$  across datasets to fixed size of: t=16, h=4 and w=4

Table 1: **Top-1 accuracies (%) of action prediction methods on UCF-101 over different observation ratios ( $\rho$ )**. Methods are grouped based on the backbone used. Best results for each feature extractor and observation ratio are underlined. The best overall performance per observation ratio is in **bold**.

Method	Features/ Backbone	dim	Observation ratios ( $\rho$ )								
			0.1	0.2	0.3	0.4	0.5	0.6	0.7	0.8	0.9
Integral BOW [46]	Hand-crafted	-	36.3	65.7	71.7	74.3	74.4	75.2	75.4	75.6	75.8
AE [7]			40.0	71.9	77.7	80.1	80.6	80.9	81.1	81.6	81.8
RGN-KF [69]	Inception [54]	2D	83.3	85.2	87.8	90.6	91.5	92.3	92.0	93.0	92.9
GGNN+LSTGCN [63]			82.4	85.6	89.0	-	91.3	-	92.4	-	93.0
TS (2xL) [59]			83.3	87.1	88.9	89.8	90.9	91.0	91.3	91.2	91.3
AAPNet [34]	C3D [55]	3D	59.9	80.4	86.8	86.5	86.9	88.3	88.3	89.9	90.9
MSSC [4]	ResNet-18	2D [22]	34.1	53.8	58.3	57.6	62.6	61.9	63.5	64.3	62.7
MTSSVM [32]			40.1	72.8	80.0	82.2	82.4	83.2	83.4	83.6	83.7
DeepSCN [33]			45.0	77.7	83.0	85.4	85.8	86.7	87.1	87.4	87.5
mem-LSTM [31]			51.0	81.0	85.7	85.8	88.4	88.6	89.1	89.4	89.7
GGNN+LSTGCN [63]			75.9	81.7	87.8	-	88.7	-	89.4	-	90.2
MSRNN [25]			68.0	87.2	88.2	88.8	89.2	89.7	89.9	90.3	90.4
<b>TemPr <math>\mathbf{\hat{L}}</math> (ours)</b>		3D [21]	<u>84.3</u>	<u>90.2</u>	<u>90.4</u>	<u>90.9</u>	<u>91.2</u>	<u>91.8</u>	<u>92.1</u>	<u>92.3</u>	<u>92.4</u>
AA-GAN [18]	ResNet-50	2D [22]	-	84.2	-	-	85.6	-	-	-	-
GGNN+LSTGCN [63]			84.1	88.5	89.8	-	90.9	-	91.4	-	91.8
TS+JVS+JCC+JFIP [15]			-	85.8	-	-	-	-	-	-	-
<b>TemPr <math>\mathbf{\hat{L}}</math> (ours)</b>		3D [21]	<u>84.8</u>	<u>90.5</u>	<u>91.2</u>	<u>91.8</u>	<u>91.9</u>	<u>92.2</u>	<u>92.3</u>	<u>92.4</u>	<u>92.6</u>
DBDNet [42]	ResNext101 [21]	3D	82.7	86.6	88.3	89.7	90.6	91.2	91.7	91.9	92.0
IGGNN+LSTGCN [62]			80.2	-	89.8	-	92.9	-	94.1	-	94.4
<b>TemPr <math>\mathbf{\hat{L}}</math> (ours)</b>			<u>85.7</u>	<u>91.4</u>	<u>92.1</u>	<u>92.7</u>	<u>93.5</u>	<u>93.9</u>	<u>94.4</u>	<u>94.6</u>	<u>94.9</u>
<b>TemPr <math>\mathbf{-}</math> (ours)</b>	X3D <sub>M</sub> [13]	3D	84.8	91.8	92.3	92.6	93.0	93.4	93.5	93.6	93.6
<b>TemPr <math>\mathbf{=}</math> (ours)</b>			85.3	92.3	92.8	93.7	93.9	93.9	94.2	94.4	94.3
<b>TemPr <math>\mathbf{\hat{L}}</math> (ours)</b>			87.4	93.3	93.9	94.4	94.0	94.2	94.4	94.9	94.9
<b>TemPr <math>\mathbf{\hat{L}}</math> (ours)</b>			<u>87.9</u>	<u>93.4</u>	<u>94.5</u>	<u>94.8</u>	<u>95.1</u>	<b>95.2</b>	<b>95.6</b>	<u>96.4</u>	<b>96.3</b>
<b>TemPr <math>\mathbf{-}</math> (ours)</b>			85.2	92.1	92.5	92.9	93.3	93.7	93.5	93.8	93.7
<b>TemPr <math>\mathbf{=}</math> (ours)</b>	MoViNet-A4 [29]	3D	85.6	92.9	93.6	94.5	94.4	94.2	94.2	94.6	94.8
<b>TemPr <math>\mathbf{\hat{L}}</math> (ours)</b>			87.3	93.1	<u>94.9</u>	94.6	95.2	94.9	94.6	95.1	95.0
<b>TemPr <math>\mathbf{\hat{L}}</math> (ours)</b>			<b>88.6</b>	<b>93.5</b>	<b>94.9</b>	<b>94.9</b>	<b>95.4</b>	<b>95.2</b>	<u>95.3</u>	<b>96.6</b>	96.2
<b>TemPr <math>\mathbf{\hat{L}}</math> (ours)</b>											

all other methods with the same ResNet-based backbones, for every observation ratio. Across our tests, the largest improvements are observed in small ratios  $0.1 \leq \rho \leq 0.3$ . With 3D ResNeXt101 [21], we achieve 85.7% for  $\rho=0.1$ , 91.4% for  $\rho=0.2$  and 92.1% for  $\rho=0.3$ , which improves the best performing prior work on the same backbone by +3.0%, +4.8% and +2.3% respectively. Similarly, when we utilize the recent MoViNet-A4 [29] as our backbone for TemPr  $\mathbf{\hat{L}}$ , we improve the accuracy, over the best reported results in prior work in each case. There are improvements of 4.5% from [63] on  $\rho=0.1$ , 5.1% from [62] on  $\rho=0.3$ , 2.3% from [62] on  $\rho=0.5$  and 3.6% from [69] on  $\rho=0.8$ . This further demonstrates that TemPr can perform favorably without a strong dependence on specific backbones.

**Something-Something (sub21)**. In Table 2a we demonstrate the class-averaged accuracy over SSsub21, with observation ratios as in [62,63]. Our pro-



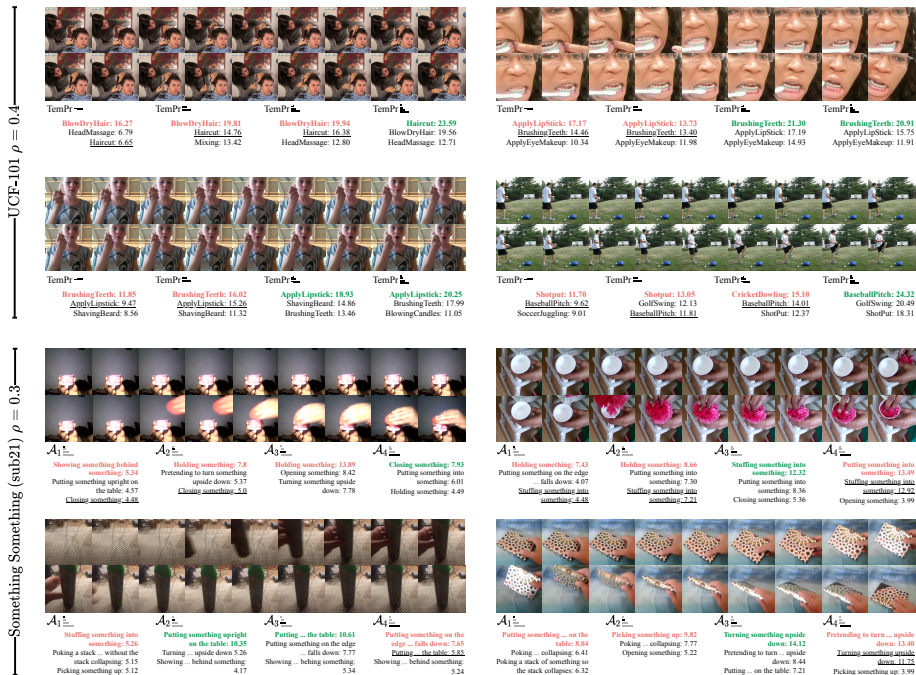


Fig. 4: **Examples from UCF-101 and SSsub21.** Top 3 action label confidences are reported for either TempPr model or over individual tower predictors ( $\mathcal{A}_i$ ). We show the 16 frames sampled per video. Green/red highlight correct/incorrect top 1 predictions, and we underline true label when in top-3. See additional examples in § S1 of the Supplementary Material.

Something that have larger temporal variations and are less appearance-based can benefit more from the proposed aggregated progressive scales. Class accuracy across scales are presented in § S2 of the Supplementary Material.

### 4.3 Ablation studies

We next conduct ablation studies on UCF-101, comparing accuracy over different observation ratios. Computations and memory usage are reported solely for TempPr, without the backbone, in order to demonstrate the differences clearer.

**Video scales strategy.** Given multiple scales, different strategies can be used for their selection. We compare our proposed temporal progressive sampling (Sec 3.2) to other common strategies and potential baselines in Table 3a. In all settings, we keep  $n = 4$  scales. The *full* strategy uses  $n$  scales of fixed length matching the entire observation video. In *equal*, scales/segments have equal lengths as in [57]. The *random* strategy uses scales of random length. Finally, the *increasing* and *decreasing* strategies utilize our proposed progressive approach, but sample the fine scale from either the start or the end of the observed video. Accuracy is consistently lower when scales are of the same length,

Table 3: Ablation studies on UCF-101 with TemPr  $\underline{\mathbf{L}}$  across obs. ratios.

(a) **Video Scales Strategy.** (b) **Accumulation function** for predictor aggregation. (c) **Weight sharing** over the attention towers and classification heads.

Scale strategy	Observation ratios ( $\rho$ )			
	0.2	0.4	0.6	0.8
full $\mathbb{I}$	86.4	88.3	88.8	89.0
equal $\mathbb{J}$	83.7	84.6	86.3	87.1
random $\mathbb{K}$	88.8	89.7	90.2	90.6
decreasing $\mathbb{L}$	90.0	<b>90.9</b>	91.6	<b>92.6</b>
increasing $\mathbb{M}$	<b>90.2</b>	<b>90.9</b>	<b>91.8</b>	92.3

Aggregation	$\rho$	
	0.2	0.4
avg	89.5	90.1
softmax	87.8	89.4
top*	84.6	87.5
gate ( $\theta=0.1$ )	85.4	88.5
ICW	89.7	90.1
<b>adaptive (<math>\mathcal{P}(\cdot)</math>)</b>	<b>90.2</b>	<b>90.9</b>

Weight sharing		$\rho$			
MAB Classifier		0.2	0.4	0.6	0.8
$\checkmark$	$\times$	73.4	76.2	79.0	79.5
$\times$	$\times$	84.7	85.8	87.3	87.8
$\times$	$\checkmark^\dagger$	83.5	84.2	85.6	87.7
$\checkmark$	$\checkmark$	89.2	90.0	90.7	91.1
$\times$	$\checkmark$	<b>90.2</b>	<b>90.9</b>	<b>91.8</b>	<b>92.3</b>

$\dagger$  w/ gradient threshold  $\theta = 1.0$ .

(d) **Number of self attention blocks (L)** w.r.t. Parameters (M), (G)FLOPs and memory use (GB). (e) **Latent array (m) sharing** over multiple towers.

L	Params (M)	FLOPs (G)	Mem. (GB)	$\rho$			
				0.2	0.4	0.6	0.8
1	20.3	1.29	2.74	70.9	74.8	80.4	86.2
2	20.6	1.32	2.78	77.2	76.3	82.8	86.7
4	21.5	1.37	2.85	83.4	84.9	85.1	87.4
6	22.2	1.42	2.93	88.7	89.5	89.8	90.1
8	23.0	1.47	3.01	<b>90.2</b>	<b>90.9</b>	<b>91.8</b>	<b>92.3</b>

m shared	Mem. (GB)	$\rho$	
		0.2	0.4
$\times$	4.015	<b>90.2</b>	<b>91.0</b>
$\checkmark$	<b>3.012</b>	<b>90.2</b>	90.9

either matching the observed video (*full*) or equally-sized (*equal*). This is in contrast to the success of this sampling approach for action recognition [57], further emphasizing the distinction between the two tasks. The use of progressive (*increasing* or *decreasing*) video scales exhibits an average +3.6% accuracy increase over different observation ratios, compared to other sampling approaches. We note that there is no architectural component that depends on the order of the scales, thus the performance over increasing or decreasing scale sizes is expected to be similar. This further emphasizes the need for fine-to-coarse sampling, independent of where the fine sample is taken from. Additional experiments for scale strategies on SSsub21 are discussed in § S3.

**Prediction accumulation.** Table 3b presents comparisons over different aggregation functions. In the case that the predictor with the highest confidence is chosen (top\*), training was done with softmax in order to ensure that gradients have been propagated for the entire network. The largest drop in performance is observed when using individual predictions (softmax, top, gate). Methods that are instead based on using all predictors either uniformly by averaging them, or by weighting them with Inverse Covariance Weighting (ICW) improve the final predictions. A further +0.7% accuracy improvement over ICW is observed by our adaptive approach with the combination of predictor agreement and confidences.

**Weight sharing combinations.** We consider the two components of the architecture that can share their weights across scales. The first is the multihead-attention blocks (MAB) and the second is their classifier layer. Table 3c shows

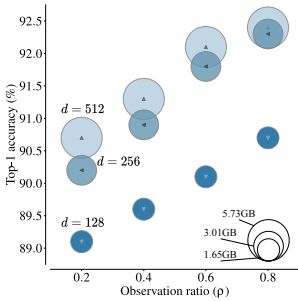


Fig. 5: **Bottleneck size** ( $d$ ) for latent array ( $\mathbf{m}$ ).

Table 4: **Ablating contributions** with individual and combined replacement.

replacement(s)			Obs. ratio ( $\rho$ )
I.	II.	III.	
$s_{1,\dots,n}$	$f(\widehat{\mathbf{z}}_i^f)$	$\mathcal{P}(f(\widehat{\mathbf{z}}_i))$	0.2 0.4 0.6 0.8
$s_n \times n$	$f(\mathbf{z}_i)$	$\overline{f(\widehat{\mathbf{z}}_i)}$	
Proposed			<b>90.2 90.9 91.8 92.3</b>
$\times$		$\times$	86.4 88.3 88.8 89.0
	$\times$		69.4 73.2 78.6 85.5
		$\times$	89.5 90.1 90.6 91.2
$\times$	$\times$		64.3 69.8 75.9 83.4
	$\times$	$\times$	67.4 72.8 77.3 84.7
$\times$		$\times$	84.2 87.0 87.4 88.3
$\times$	$\times$	$\times$	61.4 67.2 73.5 79.3

changes in the model configuration based on our contributions. Setting I. replaces the progressive scales with  $n$  copies of the observable video,  $s_{1,\dots,n} \rightarrow s_n \times n$ . In setting II. the class predictions are made from the extracted CNN features without the utilization of the attention towers  $f(\widehat{\mathbf{z}}_i^f) \rightarrow f(\mathbf{z}_i)$ . For setting III. the predictor aggregation function is replaced by averaging classifier predictions  $\mathcal{P}(f(\widehat{\mathbf{z}}_i)) \rightarrow \overline{f(\widehat{\mathbf{z}}_i)}$ . On average, a 14.63% accuracy reduction is observed across ratios when predictions are made directly from CNN features. This drop is further amplified when progressive sampling is not used, demonstrating the importance of both the proposed architecture and sub-sampling approach.

#### 4.4 Results on large-scale SSv2

In this section, we aim to investigate EAP on the large scale dataset SSv2 and explore the feasibility of utilizing the latest action recognition transformer-based models for EAP. Previous EAP works [4,3,31,33,48,59,62,63] have evaluated their performance over smaller datasets ( $< 100K$  videos) that are only partially indicative of the approaches’ generalizability. Therefore, we set a new baseline on the widely-used, large-scale and temporally challenging SSv2 dataset for EAP.

that using individual classifier weights for each tower, decreases performance. In contrast, enabling weight sharing between classifiers, to enforce a common output representation space between towers improves performance.

**Number of self attention blocks.** Table 3d demonstrates the impact of the Self MAB number on the accuracy. Increasing the number of self-attention blocks improves accuracy mostly in small observation ratios, while marginally increasing the complexity and memory requirements. We therefore adopt  $L = 8$  for our model.

**Latent array ( $\mathbf{m}$ ).** Table 3e shows the effect on both performance and memory when sharing the Cross MAB latent array  $\mathbf{m}$  across attention towers. With marginal difference in accuracy, sharing  $\mathbf{m}$  increases efficiency with a significant reduction in memory. We therefore share  $\mathbf{m}$  in all other experiments. In Fig. 5 we present performance results over different latent index dimension ( $d$ ) sizes. Size  $d = 256$  is shown to be the most cost-effective size as improvements over  $d = 128$  range between (1.1-2.3)% while requiring  $\sim 50\%$  less memory than  $d = 512$ . We use  $d = 256$  for our model. The accuracies achieved in Fig. 5 are detailed in § S4.

**Contributions ablation.** Motivated by Tables 3a and 3b, in Table 4 we present combined

Table 5: **Top-1 accuracy on large-scale Something-Something (SSv2)** based on Swin-B [39] backbone.

Method	GFLOPs	Params (M)	Obs. ratios ( $\rho$ )			
			0.1	0.3	0.5	0.7
Inference only	176.6	88.8	6.9	17.6	28.9	36.0
Fine-tuned classifier			14.4 (+7.5)	23.5 (+5.8)	31.1 (+2.2)	39.6 (+3.6)
<b>TemPr <math>\underline{\mathbf{L}}</math> (ours)</b>	178.0 (+1.4)	119.3 (+30.5)	<b>20.5</b> (+13.6)	<b>28.6</b> (+11.0)	<b>41.2</b> (+12.3)	<b>47.1</b> (+11.1)

Importantly, we wish to showcase that EAP includes challenges that are unique to this task and cannot be addressed by models trained solely for action recognition on full videos. We thus use the recently introduced Swin-B video transformer [39], due to its promising results on action recognition, and consider three settings: first, we run inference on partially observed videos with the Swin-B model trained on the full videos of SSv2. Second, we consider features from Swin-B and optimize the classifier for each observation ratio  $\rho$ . In our final setting, we use Swin-B as the backbone for our EAP-focused TemPr.

We present our large-scale results on SSv2 in Table 5. This model achieves 66.3% when evaluated on full videos (i.e.  $\rho = 1.0$ )<sup>5</sup>. We note the significant drop in performance when evaluated on partially-observed videos. Even when  $\rho = 0.7$ , the model can only achieve 36.0% top-1 accuracy. When fine-tuning these features, the improvement remains modest. The largest improvement of TemPr over the action classification Swin-B model is observed in  $\rho = 0.1$  with our TemPr  $\underline{\mathbf{L}}$  outperforming the inference only model by 13.6% and the fine-tuned model by 6.1%. Improvements are also evident across the observation ratios. This not only demonstrates the benefits of our proposed TemPr model for EAP, but also the distinction between the tasks of action classification and EAP, and thus the need for EAP-specific architectures.

## 5 Conclusions

We have proposed to utilize progressive scales from partially observed videos for early action prediction. Based on these scales, we introduce a temporal progressive (TemPr) model consisting of bottleneck-based attention towers, in order to capture the progression of an action over multiple fine-to-coarse scales. Multiple scale predictors are accumulated to a final prediction that considers the similarity in their probability distributions as well as their confidence. Extensive experiments over five backbones and three video datasets have demonstrated the merits of our approach with improvements over all previous state-of-the-art. Additionally, we have investigated the unique difficulties of EAP in large-scale settings, in comparison to action recognition models. We hope that our proposed approach utilizing progressive, rather than single continual, scales can pave a new path for subsequent methods.

<sup>5</sup> We note that the difference from the reported 69.6% accuracy in [39] is due to our use of 16 frames instead of the reported 32 frames as input.

## Data Statement

Publicly available datasets were used in this paper.

## Acknowledgments

Research funded by the United Nation’s End Violence Fund (iCOP 2.0 project) and EPSRC UMPIRE (EP/T004991/1).

## References

1. Arnab, A., Deghani, M., Heigold, G., Sun, C., Lučić, M., Schmid, C.: ViViT: A video vision transformer. In: International Conference on Computer Vision (ICCV). pp. 6836–6846 (2021)
2. Bertasius, G., Wang, H., Torresani, L.: Is space-time attention all you need for video understanding? In: International Conference on Machine Learning (ICML) (2021)
3. Cai, Y., Li, H., Hu, J.F., Zheng, W.S.: Action knowledge transfer for action prediction with partial videos. In: AAAI Conference on Artificial Intelligence. pp. 8118–8125 (2019)
4. Cao, Y., Barrett, D., Barbu, A., Narayanaswamy, S., Yu, H., Michaux, A., Lin, Y., Dickinson, S., Mark Siskind, J., Wang, S.: Recognize human activities from partially observed videos. In: Conference on Computer Vision and Pattern Recognition (CVPR). pp. 2658–2665. IEEE (2013)
5. Carreira, J., Noland, E., Banki-Horvath, A., Hillier, C., Zisserman, A.: A short note about kinetics-600. arXiv preprint arXiv:1808.01340 (2018)
6. Carreira, J., Zisserman, A.: Quo vadis, action recognition? A new model and the Kinetics dataset. In: Computer Vision and Pattern Recognition (CVPR). pp. 4724–4733 (2017)
7. Chen, M., Xu, Z., Weinberger, K.Q., Sha, F.: Marginalized denoising autoencoders for domain adaptation. In: International Conference on International Conference on Machine Learning (ICML). pp. 1627–1634 (2012)
8. Chen, Y., Fan, H., Xu, B., Yan, Z., Kalantidis, Y., Rohrbach, M., Yan, S., Feng, J.: Drop an octave: Reducing spatial redundancy in convolutional neural networks with octave convolution. In: International Conference on Computer Vision (ICCV). pp. 3435–3444 (2019)
9. Dice, L.R.: Measures of the amount of ecologic association between species. *Ecology* **26**(3), 297–302 (1945)
10. Dosovitskiy, A., Beyer, L., Kolesnikov, A., Weissenborn, D., Zhai, X., Unterthiner, T., Deghani, M., Minderer, M., Heigold, G., Gelly, S., et al.: An image is worth 16x16 words: Transformers for image recognition at scale. In: International Conference on Learning Representations (ICLR) (2020)
11. Fadiga, L., Fogassi, L., Pavesi, G., Rizzolatti, G.: Motor facilitation during action observation: a magnetic stimulation study. *Journal of neurophysiology* **73**(6), 2608–2611 (1995)
12. Fan, H., Xiong, B., Mangalam, K., Li, Y., Yan, Z., Malik, J., Feichtenhofer, C.: Multiscale vision transformers. In: International Conference on Computer Vision (ICCV). pp. 6824–6835 (2021)

13. Feichtenhofer, C.: X3D: Expanding architectures for efficient video recognition. In: Conference on Computer Vision and Pattern Recognition (CVPR). pp. 203–213 (2020)
14. Feichtenhofer, C., Fan, H., Malik, J., He, K.: SlowFast networks for video recognition. In: International Conference on Computer Vision (ICCV). pp. 6202–6211. IEEE (2019)
15. Fernando, B., Herath, S.: Anticipating human actions by correlating past with the future with jaccard similarity measures. In: Conference on Computer Vision and Pattern Recognition (CVPR). pp. 13224–13233. IEEE (2021)
16. Furnari, A., Farinella, G.M.: Rolling-unrolling lstms for action anticipation from first-person video. *IEEE Transactions on Pattern Analysis and Machine Intelligence* **43**(11), 4021–4036 (2020)
17. Gallese, V., Fadiga, L., Fogassi, L., Rizzolatti, G.: Action recognition in the premotor cortex. *Brain* **119**(2), 593–609 (1996)
18. Gammulle, H., Denman, S., Sridharan, S., Fookes, C.: Predicting the future: A jointly learnt model for action anticipation. In: International Conference on Computer Vision (ICCV). pp. 5562–5571. IEEE (2019)
19. Girdhar, R., Grauman, K.: Anticipative video transformer. In: International Conference on Computer Vision (ICCV). pp. 13505–13515. IEEE (2021)
20. Goyal, R., Ebrahimi Kahou, S., Michalski, V., Materzynska, J., Westphal, S., Kim, H., Haenel, V., Freund, I., Yianilos, P., Mueller-Freitag, M., et al.: The “something something” video database for learning and evaluating visual common sense. In: International Conference on Computer Vision (ICCV). pp. 5842–5850. IEEE (2017)
21. Hara, K., Kataoka, H., Satoh, Y.: Can spatiotemporal 3D CNNs retrace the history of 2D CNNs and ImageNet? In: Computer Vision and Pattern Recognition (CVPR). pp. 18–22 (2018)
22. He, K., Zhang, X., Ren, S., Sun, J.: Deep residual learning for image recognition. In: Computer Vision and Pattern Recognition (CVPR). pp. 770–778. IEEE (2016)
23. Hinton, G., Vinyals, O., Dean, J.: Distilling the knowledge in a neural network. In: Conference on Neural Information Processing Systems Workshops (NIPSW) (2015)
24. Hou, J., Wu, X., Wang, R., Luo, J., Jia, Y.: Confidence-guided self refinement for action prediction in untrimmed videos. *IEEE Transactions on Image Processing* **29**, 6017–6031 (2020)
25. Hu, J.F., Zheng, W.S., Ma, L., Wang, G., Lai, J., Zhang, J.: Early action prediction by soft regression. *IEEE Transactions on Pattern Analysis and Machine Intelligence* **41**(11), 2568–2583 (2018)
26. Hussein, N., Gavves, E., Smeulders, A.W.: Timeception for complex action recognition. In: Conference on Computer Vision and Pattern Recognition (CVPR). pp. 254–263. IEEE (2019)
27. Jaegle, A., Gimeno, F., Brock, A., Vinyals, O., Zisserman, A., Carreira, J.: Perceiver: General perception with iterative attention. In: International Conference on Machine Learning (ICML). pp. 4651–4664 (2021)
28. Kohler, E., Keysers, C., Umiltà, M.A., Fogassi, L., Gallese, V., Rizzolatti, G.: Hearing sounds, understanding actions: action representation in mirror neurons. *Science* **297**(5582), 846–848 (2002)
29. Kondratyuk, D., Yuan, L., Li, Y., Zhang, L., Tan, M., Brown, M., Gong, B.: Movinets: Mobile video networks for efficient video recognition. In: Conference on Computer Vision and Pattern Recognition (CVPR). pp. 16020–16030. IEEE (2021)
30. Kong, Y., Fu, Y.: Max-margin action prediction machine. *IEEE Transactions on Pattern Analysis and Machine Intelligence* **38**(9), 1844–1858 (2015)

31. Kong, Y., Gao, S., Sun, B., Fu, Y.: Action prediction from videos via memorizing hard-to-predict samples. In: AAAI Conference on Artificial Intelligence (2018)
32. Kong, Y., Kit, D., Fu, Y.: A discriminative model with multiple temporal scales for action prediction. In: European Conference on Computer Vision (ECCV). pp. 596–611. Springer (2014)
33. Kong, Y., Tao, Z., Fu, Y.: Deep sequential context networks for action prediction. In: Conference on Computer Vision and Pattern Recognition (CVPR). pp. 1473–1481. IEEE (2017)
34. Kong, Y., Tao, Z., Fu, Y.: Adversarial action prediction networks. *IEEE Transactions on Pattern Analysis and Machine Intelligence* **42**(3), 539–553 (2018)
35. Lan, T., Chen, T.C., Savarese, S.: A hierarchical representation for future action prediction. In: European Conference on Computer Vision (ECCV). pp. 689–704. Springer (2014)
36. Lee, J., Lee, Y., Kim, J., Kosiorek, A., Choi, S., Teh, Y.W.: Set transformer: A framework for attention-based permutation-invariant neural networks. In: International Conference on Machine Learning (ICML). pp. 3744–3753 (2019)
37. Li, K., Fu, Y.: Prediction of human activity by discovering temporal sequence patterns. *IEEE Transactions on Pattern Analysis and Machine Intelligence* **36**(8), 1644–1657 (2014)
38. Li, K., Hu, J., Fu, Y.: Modeling complex temporal composition of actionlets for activity prediction. In: European conference on computer vision (ECCV). pp. 286–299. Springer (2012)
39. Liu, Z., Ning, J., Cao, Y., Wei, Y., Zhang, Z., Lin, S., Hu, H.: Video swin transformer. arXiv preprint arXiv:2106.13230 (2021)
40. Ma, S., Sigal, L., Sclaroff, S.: Learning activity progression in lstms for activity detection and early detection. In: Conference on Computer Vision and Pattern Recognition (CVPR). pp. 1942–1950. IEEE (2016)
41. Meng, Y., Lin, C.C., Panda, R., Sattigeri, P., Karlinsky, L., Oliva, A., Saenko, K., Feris, R.: Ar-net: Adaptive frame resolution for efficient action recognition. In: European Conference on Computer Vision (ECCV). pp. 86–104. Springer (2020)
42. Pang, G., Wang, X., Hu, J., Zhang, Q., Zheng, W.S.: DBDNet: Learning bi-directional dynamics for early action prediction. In: International Joint Conference on Artificial Intelligence (IJCAI). pp. 897–903 (2019)
43. Park, W., Kim, D., Lu, Y., Cho, M.: Relational knowledge distillation. In: Conference on Computer Vision and Pattern Recognition (CVPR). pp. 3967–3976. IEEE (2019)
44. Qin, J., Liu, L., Shao, L., Ni, B., Chen, C., Shen, F., Wang, Y.: Binary coding for partial action analysis with limited observation ratios. In: Conference on Computer Vision and Pattern Recognition (CVPR). pp. 146–155. IEEE (2017)
45. Rizzolatti, G., Fadiga, L., Gallese, V., Fogassi, L.: Premotor cortex and the recognition of motor actions. *Cognitive brain research* **3**(2), 131–141 (1996)
46. Ryoo, M.S.: Human activity prediction: Early recognition of ongoing activities from streaming videos. In: International Conference on Computer Vision (ICCV). pp. 1036–1043. IEEE (2011)
47. Ryoo, M.S., Piergiovanni, A., Arnab, A., Dehghani, M., Angelova, A.: Token-learner: What can 8 learned tokens do for images and videos? In: Conference on Neural Information Processing Systems (NeurIPS) (2021)
48. Sadegh Aliakbarian, M., Sadat Saleh, F., Salzmann, M., Fernando, B., Petersson, L., Andersson, L.: Encouraging lstms to anticipate actions very early. In: International Conference on Computer Vision (ICCV). pp. 280–289. IEEE (2017)

49. Sermanet, P., Lynch, C., Hsu, J., Levine, S.: Time-contrastive networks: Self-supervised learning from multi-view observation. In: Conference on Computer Vision and Pattern Recognition Workshops (CVPRW). pp. 486–487. IEEE (2017)
50. Shahroudy, A., Liu, J., Ng, T.T., Wang, G.: NTU RGB+D: A large scale dataset for 3D human activity analysis. In: Computer Vision and Pattern Recognition (CVPR). pp. 1010–1019. IEEE (2016)
51. Smaira, L., Carreira, J., Noland, E., Clancy, E., Wu, A., Zisserman, A.: A short note on the kinetics-700-2020 human action dataset. arXiv preprint arXiv:2010.10864 (2020)
52. Soomro, K., Zamir, A.R., Shah, M.: UCF101: A dataset of 101 human actions classes from videos in the wild. arXiv preprint arXiv:1212.0402 (2012)
53. Stergiou, A., Poppe, R.: Adapool: Exponential adaptive pooling for information-retaining downsampling. arXiv preprint arXiv:2111.00772 (2021)
54. Szegedy, C., Liu, W., Jia, Y., Sermanet, P., Reed, S., Anguelov, D., Erhan, D., Vanhoucke, V., Rabinovich, A.: Going deeper with convolutions. In: Computer Vision and Pattern Recognition, (CVPR). IEEE (2015)
55. Tran, D., Bourdev, L., Fergus, R., Torresani, L., Paluri, M.: Learning spatiotemporal features with 3D convolutional networks. In: International Conference on Computer Vision (ICCV). pp. 4489–4497 (2015)
56. Tran, D., Wang, H., Torresani, L., Ray, J., LeCun, Y., Paluri, M.: A closer look at spatiotemporal convolutions for action recognition. In: Conference on Computer Vision and Pattern Recognition (CVPR). pp. 6450–6459 (2018)
57. Wang, L., Xiong, Y., Wang, Z., Qiao, Y., Lin, D., Tang, X., Van Gool, L.: Temporal segment networks: Towards good practices for deep action recognition. In: European Conference on Computer Vision (ECCV). pp. 20–36 (2016)
58. Wang, X., Girshick, R., Gupta, A., He, K.: Non-local neural networks. In: Conference on Computer Vision and Pattern Recognition (CVPR). pp. 7794–7803. IEEE (2018)
59. Wang, X., Hu, J.F., Lai, J.H., Zhang, J., Zheng, W.S.: Progressive teacher-student learning for early action prediction. In: Conference on Computer Vision and Pattern Recognition (CVPR). pp. 3556–3565. IEEE (2019)
60. Wu, C.Y., Feichtenhofer, C., Fan, H., He, K., Krahenbuhl, P., Girshick, R.: Long-term feature banks for detailed video understanding. In: Conference on Computer Vision and Pattern Recognition (CVPR). pp. 284–293. IEEE (2019)
61. Wu, C.Y., Li, Y., Mangalam, K., Fan, H., Xiong, B., Malik, J., Feichtenhofer, C.: Memvit: Memory-augmented multiscale vision transformer for efficient long-term video recognition. arXiv preprint arXiv:2201.08383 (2022)
62. Wu, X., Wang, R., Hou, J., Lin, H., Luo, J.: Spatial-temporal relation reasoning for action prediction in videos. *International Journal of Computer Vision* **129**(5), 1484–1505 (2021)
63. Wu, X., Zhao, J., Wang, R.: Anticipating future relations via graph growing for action prediction. In: AAAI Conference on Artificial Intelligence. pp. 2952–2960 (2021)
64. Wu, Z., Xiong, C., Ma, C.Y., Socher, R., Davis, L.S.: Adafame: Adaptive frame selection for fast video recognition. In: Conference on Computer Vision and Pattern Recognition (CVPR). pp. 1278–1287. IEEE (2019)
65. Xu, W., Yu, J., Miao, Z., Wan, L., Ji, Q.: Prediction-cgan: Human action prediction with conditional generative adversarial networks. In: International Conference on Multimedia (ACMMM). pp. 611–619 (2019)
66. Yan, S., Xiong, X., Arnab, A., Lu, Z., Zhang, M., Sun, C., Schmid, C.: Multiview transformers for video recognition. arXiv preprint arXiv:2201.04288 (2022)

67. Zhang, P., Dai, X., Yang, J., Xiao, B., Yuan, L., Zhang, L., Gao, J.: Multi-scale vision longformer: A new vision transformer for high-resolution image encoding. In: International Conference on Computer Vision (ICCV). pp. 2998–3008. IEEE (2021)
68. Zhang, Y., Li, X., Liu, C., Shuai, B., Zhu, Y., Brattoli, B., Chen, H., Marsic, I., Tighe, J.: Vidtr: Video transformer without convolutions. In: International Conference on Computer Vision (ICCV). pp. 13577–13587. IEEE (2021)
69. Zhao, H., Wildes, R.P.: Spatiotemporal feature residual propagation for action prediction. In: International Conference on Computer Vision (ICCV). pp. 7003–7012. IEEE (2019)
70. Zheng, Y.D., Liu, Z., Lu, T., Wang, L.: Dynamic sampling networks for efficient action recognition in videos. *IEEE Transactions on Image Processing* **29**, 7970–7983 (2020)
71. Zhou, B., Andonian, A., Oliva, A., Torralba, A.: Temporal relational reasoning in videos. In: European Conference on Computer Vision (ECCV). pp. 803–818 (2018)

## Supplementary material

### S1 Qualitative results over tower predictions

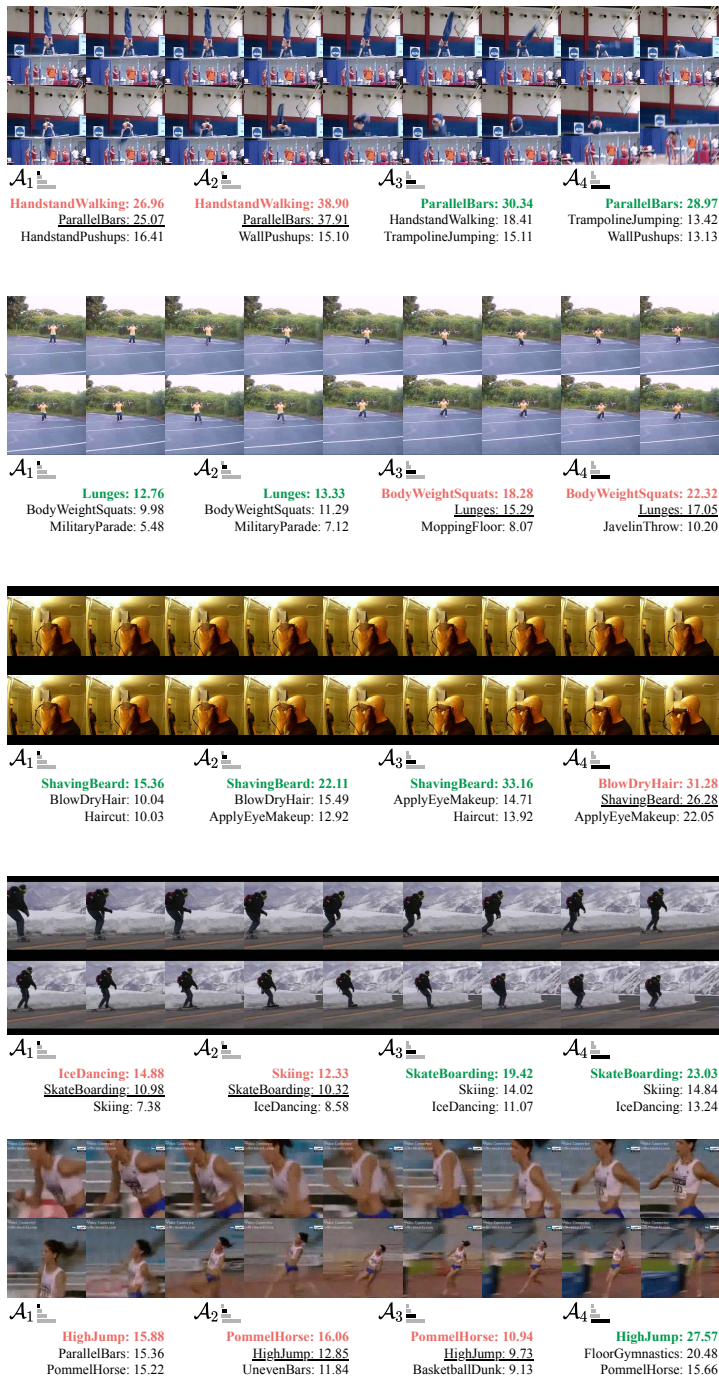
We have presented and discussed qualitative results over TemPr  $\underline{\quad}$ ,  $\underline{\quad}$ ,  $\underline{\quad}$ ,  $\underline{\quad}$  configurations and individual towers  $\mathcal{A}_1 \underline{\quad}$ ,  $\mathcal{A}_2 \underline{\quad}$ ,  $\mathcal{A}_3 \underline{\quad}$ ,  $\mathcal{A}_4 \underline{\quad}$  in Section 4.2. Here we provide additional examples in the same format of Figure 4, where predictions differ across TemPr  $\underline{\quad}$  towers.

As shown in Fig. S1, our proposed progressive scales can benefit feature modeling for a variety of action instances e.g. for the *Lunges* instance, the finer scales ( $\mathcal{A}_1 \underline{\quad}$  and  $\mathcal{A}_2 \underline{\quad}$ ) focus on smaller motions and thus are less influenced by global motion in the video. For *Lunges*, these global motions are similar to those performed for *BodyWeightSquats*. On the other hand, for the *HighJump* and *SkateBoarding* instances, coarse scales are better suited, as motions over larger temporal lengths are more descriptive of the action performed. Failure cases for coarse scales are evident in the chosen examples of *SalsaSpin*, *IceDancing* and *ShavingBeard* where motions that are descriptive for the class, are performed fast and over shorter temporal lengths.

### S2 Results for class predictions

To better understand the performance of individual towers  $\mathcal{A}_i$  with respect to the predictions made by the aggregation function  $\mathcal{P}(\cdot)$ , we study class-based accuracies on UCF-101 and SSsub21. In Fig. S2, we present accuracies for the first 30 classes on UCF-101. Overall, the performance of the aggregation function is equivalent to that of the top-performing tower. For the *BreastStroke* class, the finer scale  $\mathcal{A}_1$  outperforms other tower predictors. This is also the case for the *Billiards* class which shows a similar trend with  $\mathcal{A}_1$  achieving the best performance. We believe the high accuracy over the fine scales of both *BreastStroke* and *Billiards* classes, are due to their unique appearance and motion features. Thus, for only a small portion of the video, the ongoing action can be correctly predicted.

Class accuracies on SSsub21 are shown in Fig. S3. We observe higher variation across towers' performances comparatively to UCF-101. Overall, because of features being more motion-based compared to UCF-101, coarser scales perform better. Considering the *Putting something on the edge of something so it is not supported and falls down* class, the object will typically fall down only at the end of the action. Therefore, such information is better captured by the coarser scales. Similarly, for *Pretending to sprinkle air onto something*, *pretending* can only be captured over a longer temporal scale. Fine scales perform more favorably for shorter actions such as *Closing something*, *Picking something up* and *Turning something upside down*. For the majority of these classes, informative motions only last a few frames and are thus better addressed by finer scales.


 Fig. S1: Instances over UCF-101. Top 3 action labels are reported for  $\mathcal{A}_i$

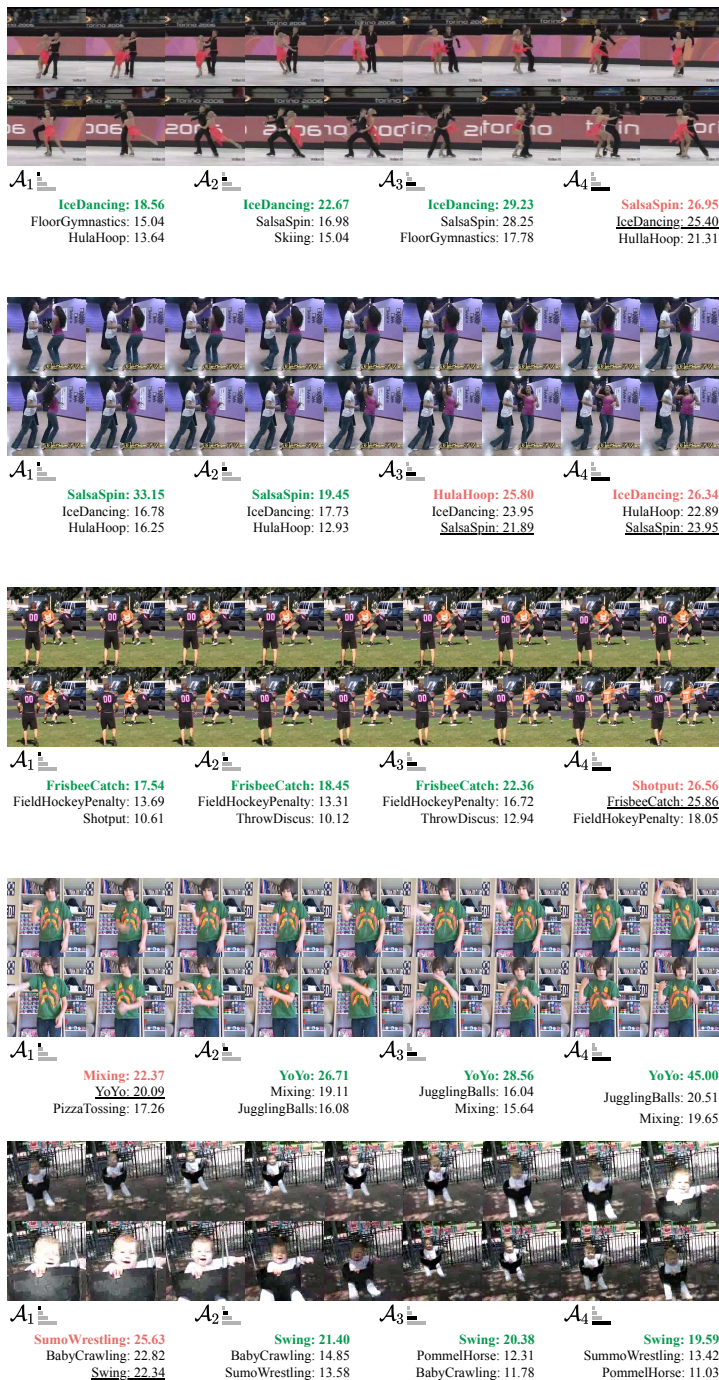


Fig. S1: Instances over UCF-101. Top 3 action labels are reported for individual tower predictors ( $\mathcal{A}$ ).

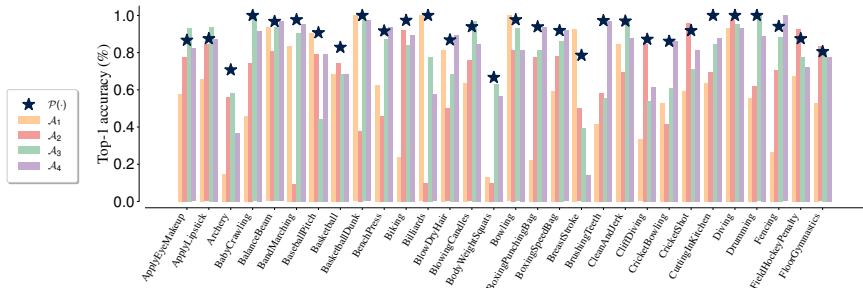


Fig. S2: UCF-101 class accuracies for the first 30 classes over observation ratio  $\rho = 0.3$ .

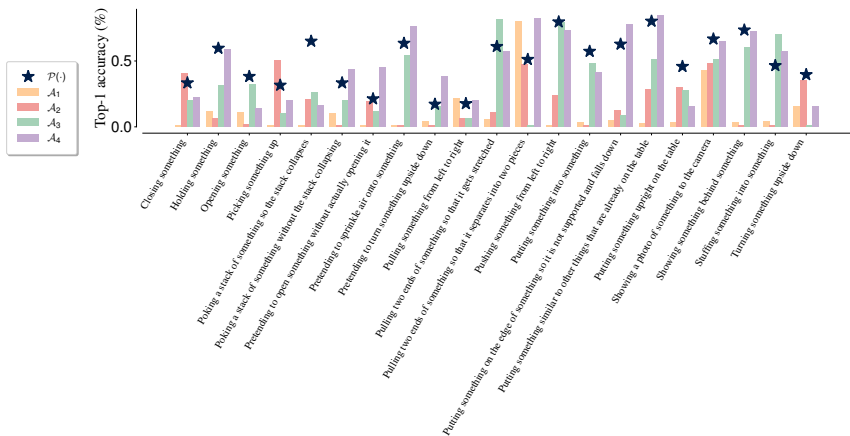


Fig. S3: SSsub21 class accuracies over observation ratio  $\rho = 0.3$ .

### S3 Video scales strategies on SSsub21

Supplementary to Table 3a, we experiment over different scale sampling strategies on SSsub21 as the dataset demonstrate more challenging temporal variations than UCF-101. We use TemPr  $\underline{\text{L}}$  with MoViNet-A4 as the backbone, matching the configurations for Table 2a. In relation to our proposed progressive *increasing* strategy, we observe the largest performance margins with the *equal* scales/segments. Decreases are in the range of 2.2% on  $\rho = 0.2$ , 3.4% on  $\rho = 0.3$ , 4.1% on  $\rho = 0.5$  and 4.0% on  $\rho = 0.7$ . This further demonstrates the contrast between the tasks of action recognition and early action prediction. The use of progressively *decreasing* scales performs on par with the *increasing* setting similar to Table 3a. Marginal improvements are observed when using progressively *decreasing* scales in smaller observation ratios and also when using progressively *increasing* scales for larger observation ratios. We believe this to be

Table S1: Video Scales Strategies on SSsub21 with TemPr  $\underline{\mathbf{L}}$ .

Scale strategy	Obs. ratios ( $\rho$ )			
	0.2	0.3	0.5	0.7
full $\equiv$	32.6	36.4	39.3	42.9
equal $\mathcal{A}$	29.8	34.5	37.2	41.8
random $\mathcal{R}$	33.4	37.1	40.6	44.3
decreasing $\mathcal{D}$	<b>35.2</b>	<b>38.3</b>	40.7	45.2
increasing $\mathcal{I}$	34.8	37.9	<b>41.3</b>	<b>45.8</b>

Table S2: Bottleneck size comparison based on latent array ( $\mathbf{m}$ ) index dimension ( $d$ ) used by the cross-attention blocks.

$d$	Mem. (GB)	Observation ratios ( $\rho$ )			
		0.2	0.4	0.6	0.8
128	1.65	89.1 (-1.1)	89.6 (-1.3)	90.1 (-1.7)	90.7 (-2.3)
256	3.01	90.2	90.9	91.8	92.3
512	5.74	<b>90.7 (+0.3)</b>	<b>91.3 (+0.4)</b>	<b>92.1 (+0.3)</b>	<b>92.4 (+0.1)</b>

primarily because EAP in the SSsub21 videos is challenging in low observation ratios.

## S4 Accuracy over bottleneck sizes

In Figure 5 we have visualized TemPr  $\underline{\mathbf{L}}$  performance on UCF-101 given different latent array  $\mathbf{m}$  sizes  $d$ . We additionally detail numerically these individual performances in Table S2. Overall  $d = 256$  demonstrates a balance between performance and memory requirements without a significant accuracy sacrifice from  $d = 512$ . In terms of memory,  $d = 128$  requires 1.36GB less than  $d = 256$ , while  $d = 512$  uses 2.73GB more.

## S5 Predictor aggregation $\beta$ values

Our proposed adaptive predictor aggregation function relies on a combination between the similarity of predictor probability distributions and their confidences. The trainable parameter of the function defined in Eq. 7 is  $\beta$  which determines the portion of  $P(\cdot)_{eICW}$  and  $P(\cdot)_{eM}$  that are used for composing the final aggregated probability distribution.

We visualize the values of the  $\beta$  parameter, for each TemPr configuration that employs multiple scales ( $\mathcal{D}$ ,  $\mathcal{I}$  and  $\underline{\mathcal{I}}$ ) across observation ratios in Fig. S4. We use the UCF-101 TemPr models with MoViNet-A4 as backbone. In general, the  $\beta$  value remains high within 0.98–0.84 for all observation ratios. A small decrease is observed in larger observation ratios, as independent predictors are

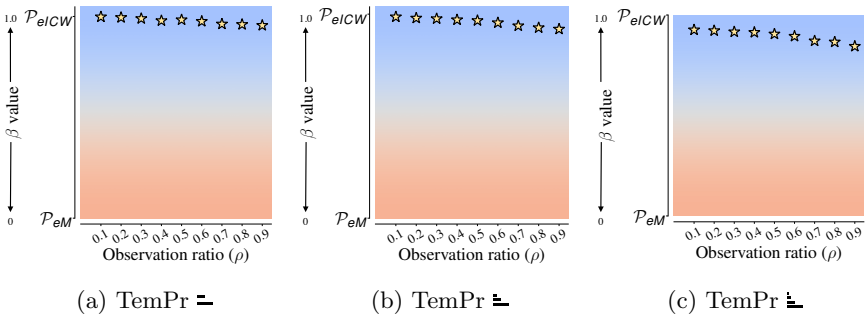


Fig. S4: **Post-training**  $\beta$  values over observation ratios on UCF-101.

exposed to larger portions of the video and are thus able to better predict the ongoing action individually.

## S6 Tower pruning

Finally, we test the generalization capabilities of each tower  $\mathcal{A}_i$  independently. We use two settings. First, we report the performance of the single-scale model TemPr - that does not include a predictor aggregation function. Instead, the tower  $\mathcal{A}_1$  from - is trained directly with Categorical Cross-Entropy (CCE). In the second setting, we select individual towers  $\mathcal{A}_i \forall i \in \mathbf{N}$  from multi-scale TemPr - . In this setting, towers predictors are trained based on the aggregation function.

We select TemPr - towers with regard to the observation ratio that they use given their scale. For example, using TemPr - trained with  $\rho = 0.4$ , and selecting predictions from tower  $\mathcal{A}_2$  - , we are effectively selecting predictions made at  $\rho_{\mathcal{A}_2} = 0.4 \cdot \frac{2}{4} = 0.2$ . Therefore, we introduce the notation  $\rho_{\mathcal{A}_i} = \rho \cdot \frac{i}{n}$  to denote the corresponding observation ratio of the *single* tower  $\mathcal{A}_i$  in relation to the *entire* video. The denoted *target* observation ratio must be equal to that of  $\rho_{\mathcal{A}_i}$  when using TemPr - and  $\rho = \rho_{\mathcal{A}_1}$  when using TemPr - .

We present our results in Table S3 where we test on 0.2 and 0.3 *target* observation ratios. As shown, the generalization capabilities of the single-scale TemPr - consistently outperform predictions from individual towers. We note that their primary difference is that predictions from towers  $\mathcal{A}_1$  - ,  $\mathcal{A}_2$  - ,  $\mathcal{A}_3$  - and  $\mathcal{A}_4$  - have been optimized based on the cross entropy from their aggregated predictions. Therefore, individual tower predictors of TemPr - demonstrate a level of specialization. Similar to the class-based trends of Fig. S2, coarse scales perform better than the finer scales.

The difference is primarily due to the aggregation function being mostly influenced by the similarity in the probability distribution of towers, as shown in Fig. S4. Considering that small observation ratios are limiting in terms of how informative their extracted features are, fine scales provide less general information than the coarser scales. Therefore, this fine-to-coarse representation

Table S3: **Inference-based TemPr** tower pruning. Results on UCF-101 when removing TemPr attention towers during inference

Target obs. ratio $\rho_{\mathcal{A}_i}$	TemPr obs. ratio $\rho$	TemPr $\mathcal{A}$	acc.
0.2	0.2	—	92.1
	0.2	$\frac{1}{2}$	86.6
	0.4	$\frac{1}{4}$	73.5
	0.8	$\frac{1}{8}$	67.1
0.3	0.3	—	92.5
	0.3	$\frac{1}{3}$	85.3
	0.4	$\frac{1}{4}$	80.5
	0.6	$\frac{1}{6}$	80.7

of the video is not effective if individual towers are to be considered separately rather than collectively.